energies

MDPI

Article

Optimized Planar Spiral Coil Design for Efficient Wireless Power Transfer in Implantable Medical Devices †

Weicheng Zhao, Yufeng Xie and Zhiyuan Chen *

State Key Laboratory of Integrated Chips and Systems, Fudan University, Shanghai 201203, China; wczhao23@m.fudan.edu.cn (W.Z.); xieyf@fudan.edu.cn (Y.X.)

* Correspondence: chen_zy@fudan.edu.cn

† This paper is an extended version of our paper published in the 2022 IEEE International Symposium on Circuits and Systems (ISCAS), Austin, TX, USA, 2022.

Abstract

This paper presents a five-coil array integrated wireless power transfer (WPT) system designed for implantable medical devices. The proposed structure features a collaborative design of driving and radiating coils, where each driving coil excites its corresponding radiating coil to emit power. All coil units are precisely tuned to operate at the 13.56 MHz ISM band. The unique array configuration generates a highly uniform magnetic field distribution within the target area, enabling excellent tolerance to lateral misalignment. System analysis based on scattering parameters (S-parameters) confirms the design's outstanding power transfer efficiency at the operating frequency. By integrating the five-coil array onto a double-layer printed circuit board, the system achieves the miniaturization and high integration level required for implantable applications. The experimental results demonstrate that the system reaches a maximum transfer efficiency of 55% under ideal alignment conditions (with a transfer distance of 10–20 mm). Notably, even with a lateral displacement of 5–10 mm at a 10 mm transfer distance, the system maintains stable performance, with efficiency consistently exceeding 50%. These results validate the system's capability for reliable and efficient wireless power delivery in clinical settings.

Keywords: wireless power transfer (WPT); 13.56 MHz; system efficiency; five-coil array; dislocation tolerance; implantable medical devices

Check for updates

Academic Editor: Salvatore Musumeci

Received: 6 February 2026
Revised: 3 April 2026
Accepted: 3 June 2026
Published: 29 June 2026

Correction Statement: This article has been republished with a minor change. The change does not affect the scientific content of the article and further details are available within the backmatter of the website version of this article.

Copyright: © 2026 by the authors. Licensee MDPI, Basel, Switzerland. This article is an open access article distributed under the terms and conditions of the Creative Commons Attribution (CC BY) license.

1. Introduction

Wireless power transfer (WPT) systems are widely used in implantable medical devices (IMDs), such as cochlear implants, retinal prostheses, and neural recording systems, as they can reduce or eliminate the need for implanted batteries [1]. However, the power transfer efficiency is significantly influenced by the coupling coefficient (k) between the transmitting (TX) and receiving (RX) coils, which is highly sensitive to their relative alignment [2,3]. In practical IMD applications, precise alignment between the TX and RX coils is often difficult to maintain. Therefore, to ensure efficient power delivery under misalignment conditions, coil structures capable of generating a uniform magnetic field are highly desirable, as they enable stable and efficient power transfer [4].

Due to the space constraints of implantable medical devices, WPT systems must be compact. Planar spiral coils (PSCs) are preferable over traditional wound coils because of their smaller size and easier integration [5]. However, a single PSC cannot produce a homogeneous magnetic flux distribution. Based on the magnetic field superposition

principle, using coil arrays with compensation structures can achieve a more homogeneous magnetic flux distribution [6].

Traditional coil designs often prioritize either miniaturization or efficiency, resulting in suboptimal performance for deep-tissue implants. For instance, tightly wound coils may exhibit reduced Q-factors due to proximity effects, while larger coils face practical limitations in integration with micro-scale IMDs. Recent advancements in multi-objective optimization algorithms, such as genetic algorithms (GAs) and particle swarm optimization (PSO), have shown promise in addressing these trade-offs. Furthermore, the adoption of biocompatible ferrite substrates has demonstrated enhanced magnetic flux concentration, improving power transfer efficiency (PTE) by up to 15% compared to air-core designs [7–10].

Because magnetic cores cannot be added between PSCs, the mutual coupling between coils remains low, leading to reduced efficiency. Nevertheless, high-frequency resonant inductive coupling techniques can mitigate this issue by improving the effective coupling between the TX and RX coils [11]. Moreover, multi-coil configurations have been shown to enhance misalignment tolerance in WPT systems [12–14]. For instance, a hybrid square array structure proposed in [3] achieves 53% efficiency under perfect alignment and 44% efficiency with a 10 mm lateral offset. Multilayer coil technology [15] and capacitance prediction using multi-cascade convolutional neural networks [16] have also been proposed to address lateral misalignment and improve WPT performance.

However, the performance of traditional PSC designs optimized in free space or saline environments will sharply decline when embedded in human tissue [17]. Experimental studies have shown that coils that achieve a power transfer efficiency (PTE) of around 50% in air can reduce their power transfer efficiency to around 20% in muscle-equivalent tissue at a working distance of 10 mm, with losses exceeding 30–40% [18–20]. This phenomenon is mainly attributed to the high dielectric constant ($\varepsilon_r \approx 50$–60) and the conductivity of biological tissue ($\sigma \approx 0.8$–1.2 S/m), which significantly changes parasitic capacitance and causes eddy current losses [21–23].

To bridge the gap between theoretical potential and clinical reality, recent research has begun integrating advanced electromagnetic modeling with structural innovation. A study demonstrated that multi-layer coil geometries can enhance magnetic flux linkage in tissue by up to 32% compared to single-layer spirals, while simultaneously reducing proximity effect losses through controlled turn spacing [24–26].

Despite these advances, a critical research gap persists: no existing design simultaneously integrates multi-layer coil geometry, explicit tissue electromagnetic modeling, and SAR-constrained co-optimization of resonant load networks into a unified framework. Most published works optimize for one criterion in isolation—either efficiency in homogeneous media, SAR reduction via structural symmetry, or coupling enhancement via metamaterials—but none holistically address the triad of challenges inherent to in vivo implantation. In addition, establishing a parasitic sensing circuit model to capture the inherent interlayer capacitance effect of double-layer coils is also crucial for coil design [27–30].

Building on these previous studies, this paper proposes a five-coil array structure operating at 13.56 MHz. The proposed design compensates for the magnetic field non-uniformity typically found in the central region of a four-coil array and fully utilizes the limited space within IMDs. This results in improved magnetic field uniformity and enhanced system efficiency. In addition, the paper introduces a novel methodology for designing coil arrays with diverse configurations to further optimize WPT performance.

The remainder of the paper is organized as follows: Section 2 provides the theoretical analysis; Section 3 introduces the proposed array structure; Section 4 presents the experimental results; Section 5 concludes the paper; and Section 6 discusses the technical implications and potential future work.

2. Theoretical Analysis

Magnetic resonance-based wireless power transfer systems are widely used in implantable medical devices. The operating frequency of such systems is restricted to the Industrial, Scientific, and Medical (ISM) bands, typically ranging from 10.4 MHz to 13.56 MHz [13]. Among these frequencies, 13.56 MHz is the most commonly used for biomedical applications. At this frequency, the wireless power transfer system can be modeled as a two-port network, as illustrated in Figure 1.

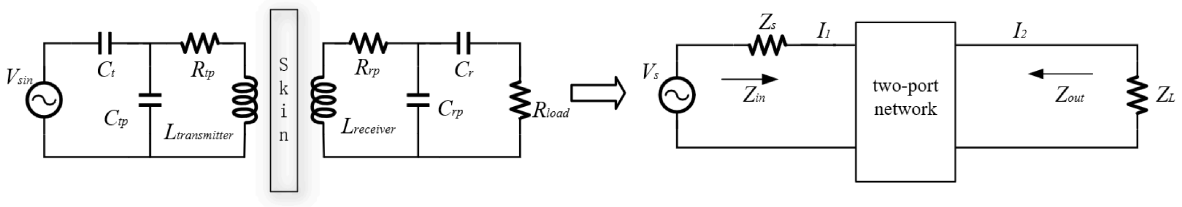


Figure 1. Implanted wireless power transfer system and its equivalent circuit.

The efficiency of a wireless power transfer system is defined as the ratio of output power to input power. In the context of the equivalent two-port network, the input power refers to the power supplied to the network from the power source, while the output power is the power delivered from the network to the load. Therefore, the efficiency can be expressed using the scattering matrix parameters. The inductive efficiency is derived as follows:

$$\eta = \frac{\left(1 - |\Gamma_G|^2\right)|S_{21}|^2\left(1 - |\Gamma_L|^2\right)}{|(1 - S_{11}\Gamma_G)(1 - S_{22}\Gamma_L) - S_{12}S_{21}\Gamma_G\Gamma_L|^2} \tag{1}$$

where η represents efficiency, S_{12} represents the reverse transmission coefficient, S_{21} represents the forward transmission coefficient, S_{11} represents the input reflection coefficient, S_{22} represents the output reflection coefficient, Γ_G represents the source reflection coefficient, and Γ_L represents the load reflection coefficient.

When the source and load are matched, there is the following relationship: $Z_G = Z_L = Z_0$. The reflection coefficient can be expressed as

$$\Gamma_L = \Gamma_G = 0, \Gamma_{in} = S_{11}, \Gamma_{out} = S_{22}$$

where Γ_{in} represents the input reflection coefficient and Γ_{out} represents the output reflection coefficient.

The expression of transfer efficiency can be expressed as

$$\eta = |S_{21}|^2 \tag{2}$$

Square coils are used in [3], but as we know, when the perimeter is equal, the area enclosed by the circle is the largest in all closed figures.

Therefore, the circular coil can maximize the limited space available in implantable medical devices. Additionally, the circular coil has no sharp angles, making it safer for the human body.

Under the same number of turns N and area A, the circular coil has a more uniform magnetic flux distribution and a shorter average loop length due to its wire distribution being closer to the ideal concentric circular current path. Therefore, according to the approximate formula:

$$L \propto \frac{\mu_0 N^2 A}{l_{avg}} \tag{3}$$

where L represents coil inductance, μ_0 represents the space permeability, N represents the number of turns, A represents the coil area, and l_{avg} represents the average length of circuit.

Its equivalent inductance value is usually slightly higher. At the same time, due to the continuous and smooth shape, the distributed capacitance C_{par} is relatively small, and the resonant frequency

$$f_0 = \frac{1}{2\pi\sqrt{LC_{total}}} \tag{4}$$

where f_0 represents resonant frequency, L represents coil inductance, and C_{total} represents total capacitance.

The resonant frequency is easier to control, and the high-frequency loss is also lower, making it highly suitable for high-frequency (>1 MHz) WPT systems, especially for implantable medical devices that require high power efficiency, small size, and tight directional tolerance. Square coils, on the other hand, can produce an electric field concentration effect at the corners, resulting in slightly larger parasitic capacitance and slightly lower inductance values. This may introduce additional losses at high frequencies, making them more suitable for mid-to-low frequency (tens to hundreds of kHz) WPT applications, especially in scenarios such as large-area power transmission boards, where they have advantages.

Due to the requirement for magnetic field strength in implanting electronic devices, the central magnetic field strength of a single coil is too strong, and the average magnetic field generated by an array coil is more advantageous.

A commonly used medical frequency is 13.56 MHz, but the frequency of 40 MHz is used in [3]. In implantable electronic devices, the resonant frequency can affect the power loss of the system. In wireless power transfer, the transmission loss in vivo is mainly related to the dielectric properties of biological tissues. According to the theory of electromagnetic wave propagation, the dielectric loss of the implant is determined by the following.

Power loss density P_L can be expressed as

$$P_L = \frac{1}{2}\sigma|E|^2 \tag{5}$$

where P_L represents the power loss density and σ represents the tissue electrical conductivity, which increases with increasing frequency. E represents the electric field intensity.

Penetration depth δ can be expressed as

$$\delta = \sqrt{\frac{2}{\omega\mu\sigma}} \tag{6}$$

where δ represents the penetration depth, ω represents the angular frequency, μ represents the magnetic permeability, and σ represents the electrical conductivity.

It can be seen from the formula that an increase in frequency ($\omega = 2\pi f$ increase) will result in a decrease in penetration depth δ and faster energy decay.

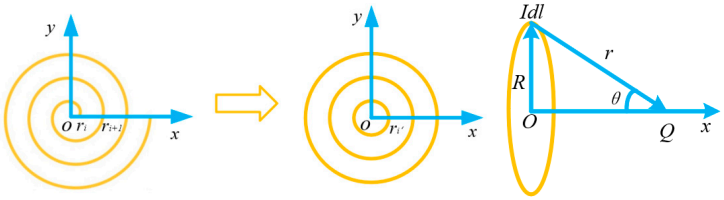
We calculated the penetration depth at different frequencies separately. After calculation, the dielectric loss at 40 MHz is about 50% higher than that at 13.56 MHz. At the same time, the penetration depth of 40 MHz is smaller (about 40% reduction), resulting in energy being more concentrated in shallow tissues. A frequency of 40 MHz results in greater transmission loss within the body. High-frequency signals can lead to more significant electromagnetic energy absorption and heat loss due to the higher conductivity and smaller penetration depth of biological tissues.

Planar spiral coils are widely used in implantable devices due to their compact design. Compared to traditional wound coils, planar spiral coils are easier to manufacture and control. According to the superposition principle of magnetic fields, the magnetic field generated by conductors of any shape can be analyzed by this principle. For closely spaced

turns, a multi-turn planar spiral coil can be considered equivalent to a concentric circle structure. As shown in Figure 2a, the radius of the *i*-th loop is given by [10].

$$r_i' = \frac{r_i + r_{i+1}}{2} \tag{7}$$

where r_i is the radius of ith turn of the planar spiral coil, r_{i+1} is the radius of $(i+1)$th turn of the planar spiral coil, and r_i' is the radius of ith turn of the equivalent coil.



(**a**) (**b**)

Figure 2. (**a**) Planar spiral coil and its equivalent model, (**b**) magnetic field generated by a circular current.

For a circular current, its magnetic field distribution can be calculated by Biot–Savart law, as shown in Figure 2b.

The magnetic flux density of a circular current B is given by

$$B = \int_0^{2\pi R} \frac{\mu_0}{4\pi} \frac{Idl \sin\theta}{r^2} \tag{8}$$

When $\sin\theta = \frac{R}{r}$, the formula can be expressed as

$$B = \frac{\mu_0 I R^2}{2(R^2 + x^2)^{\frac{3}{2}}} \tag{9}$$

For multi-turn coils, according to the superposition principle, there is

$$B = \frac{\mu_0 N I R^2}{2(R^2 + x^2)^{\frac{3}{2}}} \tag{10}$$

where R represents the radius of the circular current, x represents the vertical distance from point P to point O, N represents the number of turns, I is the amplitude of the circular current, and μ_0 is the space permeability.

In multi-coil structures, coil array is often used to generate a consistent magnetic field profile. As shown in Figure 3, due to the superposition of the magnetic field distribution, the magnetic field intensity H can be expressed as [6]

$$\begin{gathered} H_O = \sum_{i=1}^{4} \frac{NI}{4\pi} \int_0^{2\pi} \frac{\left(R^2 - y_i \cdot R \cdot \sin\theta - x_i \cdot R \cdot \cos\theta\right) \cdot d\theta}{\left[(x_i - R \cdot \cos\theta)^2 + (y_i - R \cdot \sin\theta)^2 + h^2\right]^{\frac{3}{2}}} \\ x_1 = x + \frac{d}{2}\ y_1 = y - \frac{d}{2}\ x_2 = x - \frac{d}{2}\ y_2 = y - \frac{d}{2} \\ x_3 = x + \frac{d}{2}\ y_3 = y + \frac{d}{2}\ x_4 = x - \frac{d}{2}\ y_4 = y + \frac{d}{2} \end{gathered} \tag{11}$$

where H_O represents the superposition magnetic field intensity generated by the four coils. N represents the number of the circular coil's turns, point (x_i, y_i), and i = 1,2,3,4 represents the relative position from each point on the circular current A, B, C and D to any point P in space. R represents the radius of the circular current. h represents the vertical height. θ is

the angle between position vector and coil plane. d represents the distance between the center of any two adjacent circular coils.

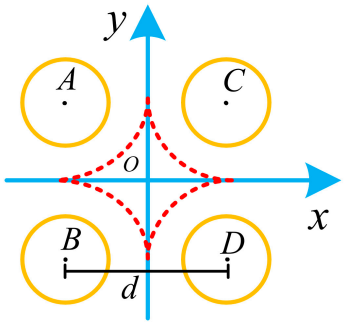


Figure 3. Four-coil structure and its equal-amplitude magnetic line distribution.

Based on numerical simulations, the magnetic field generated by a coil is typically expected to correspond to its physical shape, ensuring that the generated field is uniform and predictable. However, as shown in Figure 4, an unexpected large non-uniform region emerges at the center of the coil array. This non-uniformity in the magnetic field can be attributed to the interaction between the coils within the array. When the magnetic field is not evenly distributed, it introduces significant inefficiencies into the wireless power transfer system, particularly when the transmitting and receiving coils are not perfectly aligned. Misalignment between the coils results in a reduction in the effective coupling between them, leading to power losses, lower transfer efficiency, and potential operational instability. These inefficiencies can hinder the performance of the system, especially in practical applications where precise alignment cannot always be guaranteed.

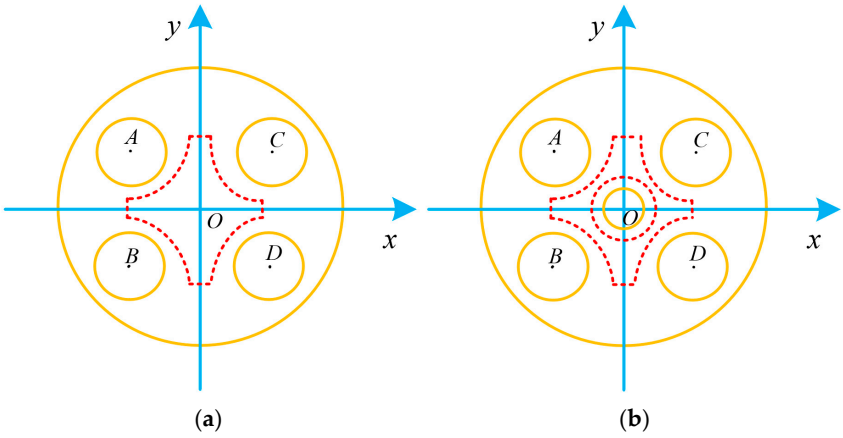


Figure 4. (**a**) Four-coil united structure and its equal-amplitude magnetic line distribution, (**b**) after adding compensation coils and its equal-amplitude magnetic line distribution.

To address this issue, one potential solution is to introduce a larger coil around the periphery of the coil array. The addition of this larger coil helps to modify the magnetic field distribution and mitigate the unevenness observed at the center. This adjustment reduces the central region's non-uniform magnetic field, leading to a more uniform and balanced field throughout the array. By improving the symmetry of the magnetic field, the overall power transfer efficiency can be enhanced, ensuring that the system remains effective even when slight misalignments occur.

The distribution of magnetic lines with equal amplitude can be calculated using a theoretical model, which provides insight into how the field behaves with the new configuration. As shown in Figure 4a, the theoretical model predicts the improved magnetic field distribution, with a more balanced field that minimizes the non-uniform region at

the center of the array. This uniformity enhances the power transfer efficiency, making the system more robust and resilient to misalignment. The theoretical model serves as a valuable tool for optimizing the design of coil arrays in wireless power transfer systems, helping to achieve high efficiency even under varying real-world conditions.

$$H_S = H_O + H_L \tag{12}$$

$$H_L = \frac{I}{4\pi}\int_0^{2\pi} \frac{({R_L}^2 - y \cdot R_L \cdot \sin\theta - x \cdot R_L \cdot \cos\theta) \cdot d\theta}{\left[(x - R_L \cdot \cos\theta)^2 + (y - R_L \cdot \sin\theta)^2 + h^2\right]^{\frac{3}{2}}} \tag{13}$$

where H_L represents the magnetic field intensity generated by the peripheral large coil, H_S represents superimposed magnetic field strength, R_L represents the radius of the peripheral circular current, (x, y) represents point P coordinates, θ represents the angle of the position vector, I represents the amplitude of the circular current, and h represents the vertical height.

After adding a large coil at the periphery, the magnetic field uniformity of the entire coil array improves, as shown in Figure 4a. If an additional coil unit is placed in the center of the array, it can help compensate for the uneven magnetic field in the middle, as shown in Figure 4b.

By placing a small coil in the center of a four-coil array, the uneven magnetic field in the array can be further compensated, as depicted in Figure 4b. According to previous theoretical analysis, the magnetic field generated by the coil should correspond to its shape.

If the size of the compensating coil differs from the coil unit in the four-coil array, as shown in the magnetic line distribution in Figure 4b, the non-uniform magnetic field area in the center will not be fully compensated. If the compensating coil is larger than the coil unit of the array, a new non-uniform magnetic field region will be generated.

Therefore, it is optimal for the compensating coil to have the same size as the coil unit in the four-coil array, as shown in Figure 5a.

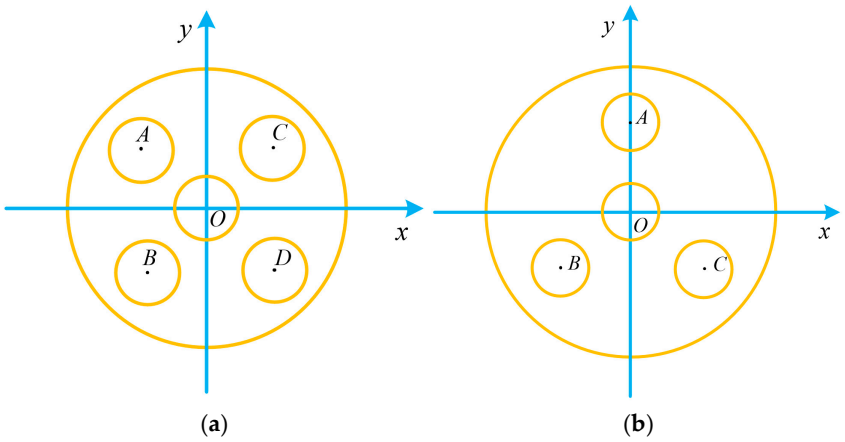


Figure 5. (**a**) Proposed equivalent five-coil united structure, (**b**) three-coil array equivalent structure.

We can discuss other shapes of coil arrays, the formation of magnetic fields, and the generation of magnetic field distributions. To verify the superiority of our designed coil array performance, we choose two other coil array structures to compare with our proposed coil array.

When using three external coils, as depicted in Figure 5b, the overall structure is simpler and can effectively save space, making it suitable for applications where space is limited and cost-sensitive. However, the magnetic field distribution in a three-coil system may not be as uniform as in systems with more coils. In cases of misalignment between

the transmitting and receiving coils, this could lead to significant energy losses, thereby reducing the efficiency of wireless power transfer. Therefore, although a three-coil system can reduce the complexity of design and production, its fault tolerance is relatively poor when misalignment occurs, and the transmission efficiency may be limited.

In contrast, the use of five or more external coils enhances magnetic field uniformity, especially under conditions of misalignment between the transmitting and receiving coils, as depicted in Figure 6. The additional coils can effectively compensate for the magnetic field inhomogeneity caused by misalignment, thus enhancing the system's transmission efficiency. Furthermore, the five-coil design increases the system's tolerance to errors, making it more stable in practical applications. Although a five-coil structure increases design complexity and cost, it provides a more ideal solution for applications that demand higher efficiency and fault tolerance.

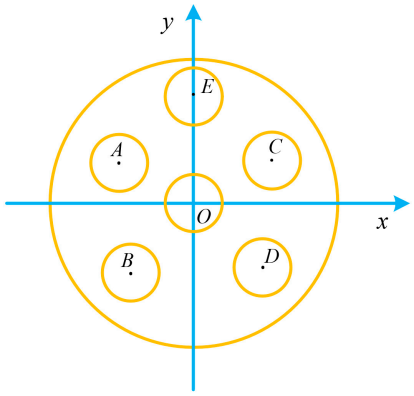


Figure 6. Six-coil array equivalent structure.

3. Proposed Array Structure

Based on the theoretical analysis of the previous chapters, a five-coil array which can produce consistent magnetic field profile is designed, as shown in Figure 7. It can improve dislocation tolerance and the efficiency of the wireless power transfer systems.

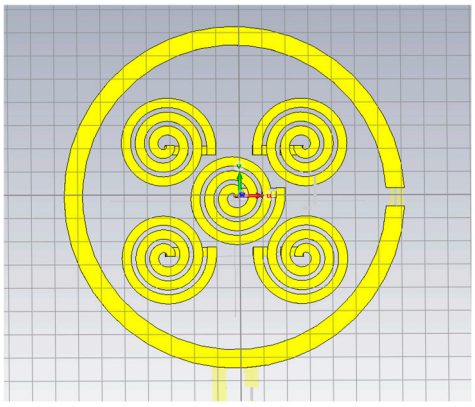


Figure 7. Proposed five-coil united planar spiral coil.

As shown in Figure 7, the five-coil united planar spiral coil is composed of five identical three-turn coils, all of which are encircled by a larger coil. This configuration is designed to optimize the efficiency of the wireless power transfer system. The radiating coils, which are responsible for emitting the power, are driven by the bottom driving coils. Both the radiating and driving coils are specifically designed to resonate at a frequency of 13.56 MHz, which is a common operational frequency for biomedical applications. This resonance ensures that the coils are operating at the same frequency point, thus effectively

concentrating the power at the resonant frequency. The resulting concentration of energy minimizes power losses and enhances the overall efficiency of the system. Additionally, this resonance at 13.56 MHz not only reduces energy losses but also helps maintain stability during power transfer, ensuring consistent and reliable energy delivery.

In terms of designing the size of the coil array, we use an iterative algorithm. We design five circular spiral coils with a coil spacing of D = 10 mm and a load of RL = 50 Ω. The iterative steps are as follows:

(1) Enter initial value.
(2) Calculate efficiency by inputting formulas.
(3) Has the calculation efficiency value improved?
(4) If increased, the relevant parameters will increase or decrease in a positive direction.
(5) If there is no improvement, then increase or decrease the relevant parameters in reverse.

The design parameters of the final single-coil unit are as follows:

We use the coil size calculated by iterative algorithm as the size of the simulation coil for simulation design. As shown in Table 1.

Table 1. Design parameters of a single-coil unit.

Design Parameters	Numerical Value	Parameter Characteristics
N	3	number of turns
d	1 mm	turn spacing
W	2 mm	line width

The same design principle applied to the transmitting coil is also extended to the receiving coil. The receiving coil is designed to match the resonant frequency of the transmitting system, ensuring that it can efficiently capture the power being transmitted without significant energy loss. By aligning the resonance of both the transmitting and receiving coils at the same frequency, the system is optimized for maximum power transfer efficiency.

Building on the theoretical analysis presented in the previous chapter, the five-coil united planar spiral coil can be understood as a system of five LC resonant circuits. Each of these individual circuits resonates in conjunction with the LC equivalent resonant circuit of the transmitting coil, facilitating effective power transfer. As shown in Figure 8, this resonant configuration allows for the efficient coupling of power from the transmitting coil to the receiving coil through the mutual resonance of all five circuits. Each of the LC circuits in the five-coil structure operates in harmony with the others, ensuring that the energy transfer is maximized, while minimizing losses that typically occur due to mismatched resonances or frequency discrepancies.

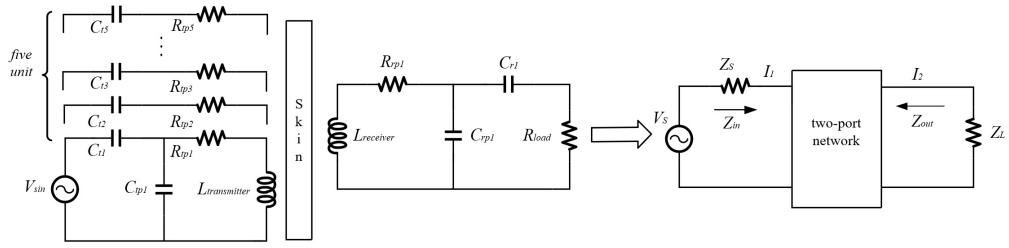


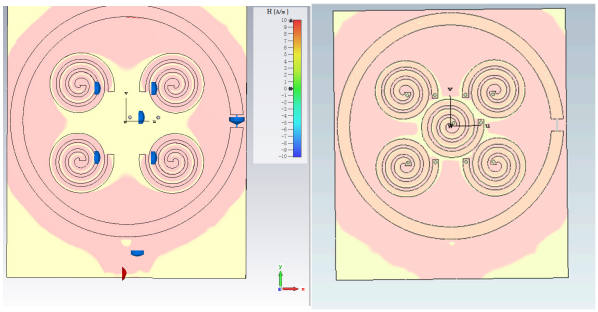
Figure 8. Proposed equivalent five-coil united structure.

The careful design and analysis of these LC resonant circuits, particularly their resonance frequencies and coupling factors, play a critical role in ensuring the optimal operation of the wireless power transfer system. This approach allows for better control of the mag-

netic field distribution and ensures that the power is transferred with minimal interference or loss, enhancing the overall performance of the system, especially in applications such as implantable medical devices where efficient and reliable power transfer is essential.

Due to the small inductance value of the planar spiral coil, the inductance value of the transmitting coil unit is about 1 μH, and the resonant frequency is 13.56 MHz. Therefore, in the simulation setting, the capacitance value corresponding to the transmitting coil unit is 137.76 pF. That is, the capacitance value of the resonant capacitors C1 to C5 corresponding to the transmitting coil unit is 137.76 pF. The inductance value of the receiving coil is about 0.5 μH, and the corresponding resonant capacitance value is 275.52 pF.

The magnetic fields of the four-coil united structure and five-coil united structure are analyzed respectively in magnetic field simulation software CST Studio Suite 2020 with setting 5 V and 0.5 A excitation; their radiation power distributions are shown in Figure 9.



(**a**) (**b**)

Figure 9. (**a**) Four-coil united structure magnetic field distribution, (**b**) five-coil united structure magnetic field distribution.

As shown in Figure 9a, a significant uneven magnetic field distribution is present in the center of the four-coil united structure. This non-uniform region is particularly evident and its shape closely aligns with the uneven area predicted by the theoretical analysis presented in the previous chapter. The existence of such non-uniform regions can negatively impact the efficiency of wireless power transfer, as the misalignment between the transmitting and receiving coils can lead to power loss and reduced system performance. This theoretical insight highlights the importance of optimizing coil configurations to minimize such non-uniformity.

To address this issue, a coil of equal size was added at the center of the array. The introduction of this compensatory coil effectively mitigates the uneven magnetic field distribution in the middle of the coil array. The result is a more uniform magnetic field across the entire coil array, which significantly enhances the efficiency of the power transfer process. As shown in Figure 9b, the five-coil united structure demonstrates an excellent compensation effect, where the previously uneven magnetic region is nearly entirely corrected. The range of magnetic field strength is between 5 A/m–6 A/m. The five-coil array structure achieves almost uniform magnetic field strength. This compensation not only improves the uniformity of the magnetic field but also ensures more efficient energy transfer between the coils, even in cases of slight misalignment.

The addition of the compensatory coil optimizes the overall system performance by reducing the areas of magnetic field non-uniformity and minimizing power loss, thus providing a more reliable and efficient wireless power transfer system. The five-coil structure with compensation is a promising solution for improving the power transfer efficiency in implantable medical devices and other wireless power applications.

The proposed five-coil array structure is designed and implemented by CST simulation software. All coils are implemented on FR4 substrate (ε_γ = 4.4, tanδ = 0.02, thickness 1 mm).

At 13.56 MHz, the dielectric constant of muscle tissue σ is 0.8 S/m. Therefore, in the simulation design optimization of the coil, we use a conductivity of 0.8 S/m as the dielectric parameter value between the transmitting coil and receiving coil. The system simulation is shown in Figure 10.

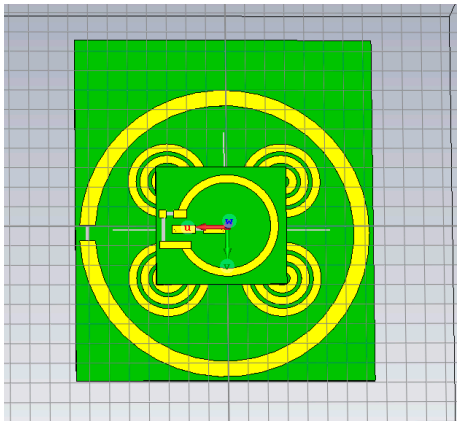


Figure 10. 3D planar spiral coil model constructed in CST Studio Suite 2020 simulation software.

The TX and RX coil models are simulated. Because the coil itself has inductance, every coil unit of the coil array connected with a capacitor can resonate. Changing the capacitance value can make the system resonate at 13.56 MHz, as shown in Figures 10 and 11.

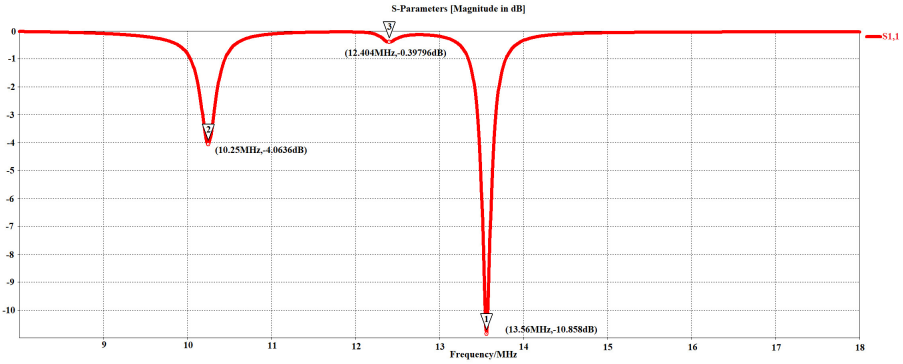
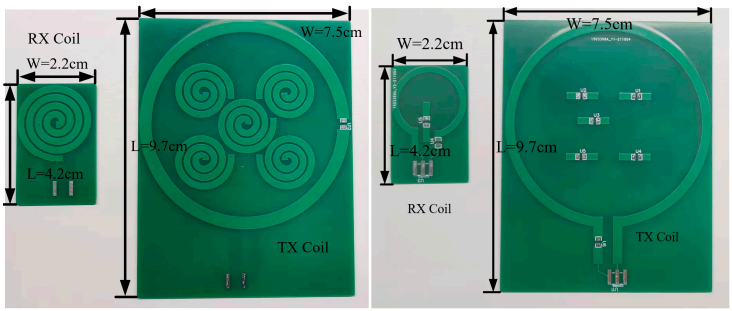


Figure 11. Simulation result of S11 parameter.

As can be seen from Figure 11, there are two resonance points in the WPT system, but the resonance depth of the resonance point at 13.56 MHz is much greater than the other, which makes the energy more concentrated at 13.56 MHz and realizes efficient power transfer.

The TX coil and RX coil are fabricated, as shown in Figure 12. The volume of the implants is less than 40 mm × 40 mm × 10 mm, so the maximal size of the RX coil is 30 mm. In this design, a 28 mm diameter spiral coil is used. And the TX coil diameter is 74 mm. The whole structure is compact. The array coil is a transmitting coil located outside the body and does not require implantation inside the body. So, using FR4 substrate material is in line with the design requirements. The coil implanted in the human body can be replaced by medical silicone-encapsulated flexible circuits, PEEK, and other alternatives. However, considering the performance verification of the coil, we have used FR4 substrate as the substrate for coil manufacturing for both the transmitting coil and the receiving coil.



(**a**) (**b**)

Figure 12. Fabricated TX and RX coils: (**a**) top view, (**b**) bottom view.

4. Experimental Results

The WPT system is built and tested. In order to truly simulate the working environment of the implanted devices, sliced pork is used to simulate the implanted human tissue, and a vector network analyzer (R&S ZVA50, Rohde & Schwarz GmbH & Co. KG, Munich, Germany) is used to measure the system scattering parameters, as shown in Figure 13.

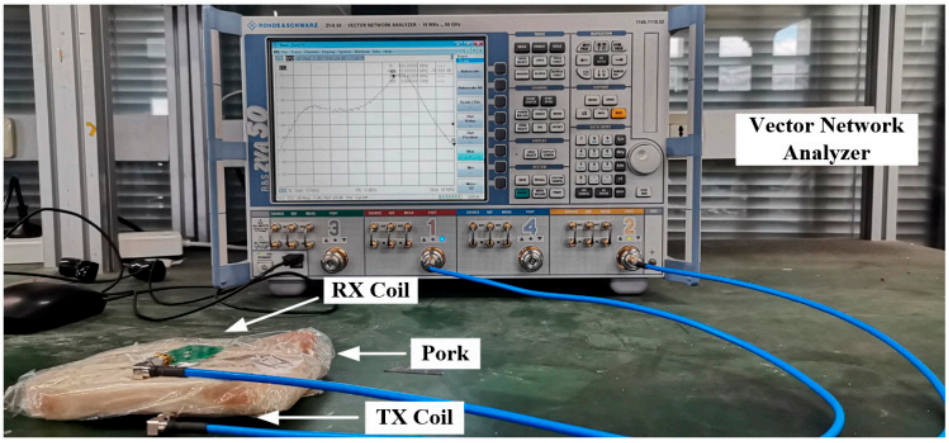
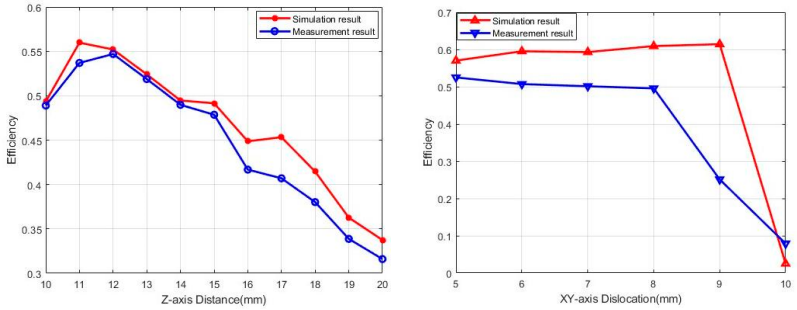


Figure 13. The experimental system for simulating implanted device.

The proposed coil structure was tested in vitro by simulating the human body. Sliced pork tissue is widely adopted in ex vivo dielectric studies as a surrogate for human soft tissues due to its comparable dielectric properties across the 100 MHz–10 GHz range, particularly in muscle-like and organ-mimicking samples. To minimize dehydration-induced drift, all measurements were conducted under controlled environmental conditions. Samples were measured within 30 min of excision to limit water loss. The experimental results are compared with the simulation results obtained in the previous chapter. And they are divided into the following cases.

The system operates within the frequency range of 8–18 MHz, determined from VNA measurements of the driver coil 's input reflection coefficient under nominal load conditions. This range ensures efficient power transfer across all receiver positions, as validated in Section 4. The measured Q-factor of a single transmitting coil is Q_1–$Q_5 \approx 170$, and the measured Q-factor of a receiving coil is $Q_6 \approx 56$. These measurements were obtained using a network analyzer, ensuring consistency with the system's operational parameters.

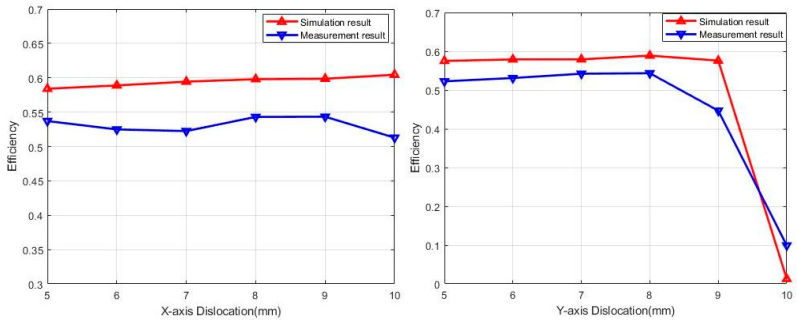
When the TX coil and RX coil are fully aligned, the distance between the coils are changed from 10 mm to 20 mm to obtain the system efficiency of WPT, as shown in Figure 14a.



(**a**) (**b**)

Figure 14. (**a**) Efficiency for the case of z-axis distance changes. (**b**) Efficiency for the case of xy-axis dislocation.

Similarly, the Z axis is kept at 10 mm and the distances of the X axis, Y axis and XY axis are changed, respectively. The calculated system efficiencies are shown in Figures 14b and 15a,b.

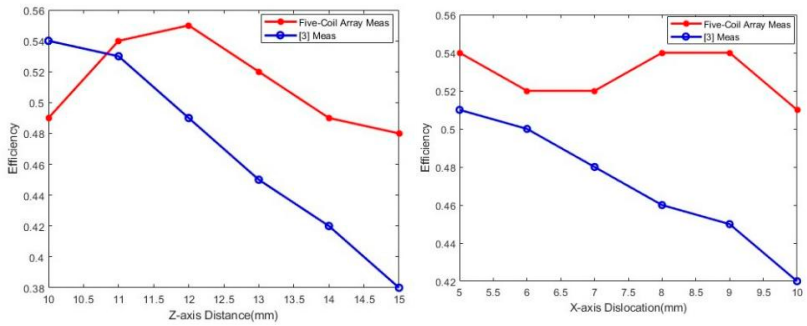


(**a**) (**b**)

Figure 15. (**a**) Efficiency for the case of x-axis dislocation. (**b**) Efficiency for the case of y-axis dislocation.

From Figure 14a, it can be seen that the trend of simulation results is basically consistent with the experimental results. When the distance is 12 mm, the efficiency reaches 55%. Most efficiencies are above 40%. From Figures 14b and 15a,b, the variation in efficiency with distance would not exceed 4% except at a few points. And most efficiencies are above 50%.

Comparing this work with reference [3], it was found that there is a significant improvement in the performance of wireless power transfer systems. Under the alignment condition, changing the vertical distance between the transmitting coil and receiving coil compares with the efficiency in [3], as shown in Figure 16a.



(**a**) (**b**)

Figure 16. (**a**) Efficiency contrast for the case of z-axis dislocation. (**b**) Efficiency contrast for the case of x-axis dislocation.

From Figure 16a, we can see that as the vertical distance gradually increases, the efficiency of the proposed five-coil array structure is significantly improved compared to reference [3].

Similarly, when there is a displacement between the transmitting coil and receiving coil, the five-coil array structure can also maintain high power transfer efficiency, as shown in Figures 16b and 17.

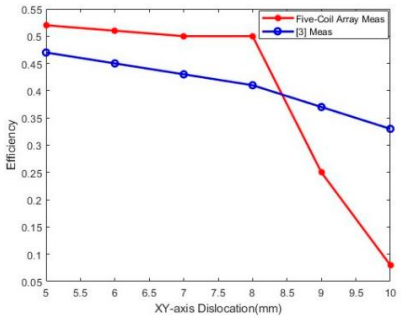


Figure 17. Efficiency contrast for the case of xy-axis dislocation.

For a better understanding of the presented results, the dislocation tolerance factor g is introduced:

$$g = \frac{|\eta_2 - \eta_1|}{d_x^2 + d_y^2} \times 10^2 \tag{14}$$

where η_1, η_2 are the efficiency values, and d_x, d_y are the offset distances between the RX coil and the center of the TX coil.

It can be seen from the definition that the smaller the value of g, the better the dislocation tolerance of the system. Through calculation, the g values of all efficiency data groups are less than 0.5. More intuitively, it can be seen from the efficiency line charts that with the change in position, the efficiency is mostly at 50–55% (except at a few points). Compared with peers, this work is also greatly improved, as shown in Table 2.

Table 2. Comparison with previously published works.

	Frequency	Dimension of Receiver	d_p	η_{max}	Input Power	Maximum Offset
[2]@Air	13.56 MHz	40 × 40 mm^2	78 mm	41%	0.5 W	N/A
[3]@IMD	40 MHz	10.3 × 10.6 mm^2	10 mm	53.3%	1 W	10 mm
[5]@IMD	13.56 MHz	10 × 10 mm^2	10 mm	21.8%	N/A	10 mm
[11]@Air	145 kHz	45.3 × 45.3 mm^2	7 mm	46.1%	N/A	25 mm
[12]@Air	13.56 MHz	132 × 132 mm^2	75 mm	53%	N/A	N/A
This work@IMD	13.56 MHz	30 × 30 mm^2	10 mm	55%	2.5 W	10 mm

5. Safety Considerations for Implanted Devices

Regarding safety considerations, IEEE establishes fundamental limitations on human body energy absorption through the Specific Absorption Rate (SAR). The SAR is defined as

$$SAR = \frac{\sigma |E|^2}{\rho} \tag{15}$$

where σ is the conductivity of the tissue, ρ is the density of the tissue, and E is the root-mean-square electric field strength in tissue.

According to the IEEE standard C95.1-2019, the SAR averaged over 1 g of cubic tissue (1 g average SAR) has to be less than 1.6 W/kg to preserve the safety of the human

body and the SAR averaged over 10 g of cubic tissue (10 g average SAR) should be less than 2 W/kg [17]. Therefore, the compliance of the proposed link with safety regulations was verified using CST Studio Suite 2020 software. In a simulation environment that approximates the human body, the simulation results meet expectations. Standardized SAR measurements were conducted according to the IEEE C95.1-2019 protocol. The maximum peak spatial SAR value (average over 1 g) at the nearest tissue interface is 0.78 W/kg, far below the common exposure limit of ICNIRP 2.0 W/kg.

The frequency of 13.56 MHz resides in the internationally recognized Industrial, Scientific, and Medical (ISM) band (IEEE Std 802.15.6) [30], ensuring regulatory compliance and interoperability with existing biomedical devices. Lower kHz-range frequencies lack standardized power/emission regulations for medical applications.

The wavelength at kHz frequencies (e.g., 22 km at 13.56 kHz) would require impractically large antennas (>10 cm diameter) for adequate near-field coupling, incompatible with implantable device dimensions. At 13.56 MHz, $\lambda/4$ is 5.5 m in air, but effective miniaturization to <2 cm is achievable through spiral coil design.

The selection of 13.56 MHz is based on the above key considerations that balance SAR reduction and practical implementation requirements.

6. Conclusions

In this paper, a five-coil array integrated structure for wireless power transfer (WPT) in implantable medical devices is proposed. All coils are fabricated on a planar printed circuit board and precisely tuned to resonate at 13.56 MHz. The coil array is designed to generate a near-uniform magnetic field distribution, thereby significantly enhancing the system's tolerance to lateral misalignment. Both simulation and experimental results verify the system's effectiveness. The maximum power transfer efficiency reaches 55% at transfer distances ranging from 10 mm to 20 mm. Even under lateral displacements of 5 mm to 10 mm along the X, Y, and XY axes, the system maintains peak efficiency above 54%. Furthermore, efficiency remains above 50% for transfer distances under 14 mm and displacements less than 8 mm. The proposed five-coil array structure demonstrates improved efficiency and robustness, making it well-suited for reliable wireless power delivery in biomedical applications.

7. Discussion

Although the proposed five-coil array structure has demonstrated notable improvements in wireless power transfer (WPT) efficiency, several important aspects remain to be addressed for further advancement. One key limitation is the system's reliance on a fixed resonant frequency (13.56 MHz), which restricts its adaptability to other operating frequencies or application scenarios that may require frequency agility. But the selection of 13.56 MHz is not arbitrary—it is the result of rigorous physical optimization. Lower or higher frequencies do not enhance safety; they compromise system feasibility and may inadvertently increase thermal risk. Moreover, the current design of the receiving coil, while functional, has not been fully optimized for the stringent spatial constraints of implantable medical devices. Enhancing the miniaturization and biocompatibility of the receiving coil remains a critical challenge. In summary, both the transmitting and receiving coil designs offer significant potential for further optimization in terms of frequency flexibility, spatial efficiency, and system integration—paving the way for more versatile and practical WPT solutions in biomedical applications.

In addition, although the coil array we designed is for implantable electronic devices, the design principles and methods described in the paper can be applied to non-invasive wireless charging frameworks in the future. Under the high power transmission distance

applied by high-clearance electric vehicles, the system may not be interoperable, especially considering the misalignment between the transmitter and receiver and the limited installation space allowed in electric vehicles. To address these challenges, the design principles and methods proposed in this work, as well as the coil array structure, can be applied to non-invasive system frameworks in vehicle chargers, enabling seamless integration into electric vehicles and maintaining high efficiency under severe coupling constraints. This provides a scalable approach for the safe and compatible deployment of wireless electric vehicle charging (WEVC) in real electric vehicle fleets.

Author Contributions: Conceptualization, W.Z. and Z.C.; methodology, Y.X.; software, W.Z.; validation, Z.C., Y.X. and W.Z.; formal analysis, W.Z.; investigation, W.Z.; resources, Z.C.; data curation, W.Z.; writing—original draft preparation, W.Z.; writing—review and editing, Z.C.; visualization, W.Z.; supervision, Z.C.; project administration, Y.X.; funding acquisition, Z.C. All authors have read and agreed to the published version of the manuscript.

Funding: This work was supported by the Joint R&D Fund of Beijing Smartchip Microelectronics Technology Co., Ltd. under Grant SGSCDT00MNQT2500130.

Data Availability Statement: The original contributions presented in this study are included in the article. Further inquiries can be directed to the corresponding author.

Conflicts of Interest: The authors declare no conflict of interest.

References

1. Li, X.; Tsui, C.-Y.; Ki, W.-H. A 13.56 MHz Wireless Power Transfer System With Reconfigurable Resonant Regulating Rectifier and Wireless Power Control for Implantable Medical Devices. In Proceedings of the 2014 Symposium on VLSI Circuits Digest of Technical Papers, Honolulu, HI, USA, 10–13 June 2014.
2. Jow, U.-M.; Ghovanloo, M. Geometrical Design of a Scalable Overlapping Planar Spiral Coil Array to Generate a Homogeneous Magnetic Field. *IEEE Trans. Magn.* **2013**, *49*, 2933–2945. [CrossRef]
3. Wang, Q.; Che, W.; Mongiardo, M.; Monti, G. Wireless Power Transfer System With High Misalignment Tolerance for Bio-Medical Implants. *IEEE Trans. Circuits Syst. II Express Briefs* **2020**, *67*, 3023–3027. [CrossRef]
4. Zhao, W.; Mai, S. Design of High Efficiency Planar Spiral Coil for Implantable Wireless Power Transfer Systems. In Proceedings of the 2022 IEEE International Symposium on Circuits and Systems (ISCAS), Austin, TX, USA, 27 May–1 June 2022.
5. Jow, U.; Ghovanloo, M. Modeling and Optimization of Printed Spiral Coils in Air, Saline, and Muscle Tissue Environments. *IEEE Trans. Biomed. Circuits Syst.* **2009**, *3*, 339–347. [CrossRef]
6. Zhang, C.; Wang, W.; Xu, C.; Yang, J. Research on Uniform Magnetic Field Compensation Structure of Array Circular Coils for Wireless Power Transfer. *IEEE Trans. Magn.* **2021**, *57*, 8600205. [CrossRef]
7. Kim, D.; Jeong, D.; Kim, J.; Kim, H.; Kim, J.; Park, S.-M.; Ahn, S. Design and Implementation of a Wireless Charging-Based Cardiac Monitoring System Focused on Temperature Reduction and Robust Power Transfer Efficiency. *Energies* **2020**, *13*, 1008. [CrossRef]
8. Zou, Y.; Liao, H.-C.; Wang, W.; Kim, W.; Su, Y.; Robinson, J.T.; Yang, K. An Efficient Power Management Unit With Continuous MPPT and Energy Recycling for Wireless Millimetric Biomedical Implants. *IEEE J. Solid-State Circuits* **2026**, *61*, 925–936.
9. Jeon, S.-J.; Seo, D.-W. Effect of Additional Transmitting Coils on Transfer Distance in Multiple-Transmitter Wireless Power Transfer System. *IEEE Access* **2022**, *10*, 9174–9183. [CrossRef]
10. Omi, A.I.; Jiang, A.; Chatterjee, B. Efficient Inductive Link Design: A Systematic Method for Optimum Biomedical Wireless Power Transfer in Area-Constrained Implants. *IEEE Trans. Biomed. Circuits Syst.* **2025**, *19*, 300–316. [CrossRef] [PubMed]
11. Achterberg, J.; Lomonova, E.A.; de Boeij, J. Coil Array Structures Compared for Contactless Battery Charging Platform. *IEEE Trans. Magn.* **2008**, *44*, 617–622. [CrossRef]
12. RamRakhyani, A.K.; Lazzi, G. Multicoil Telemetry System for Compensation of Coil Misalignment Effects in Implantable Systems. *IEEE Antennas Wirel. Propag. Lett.* **2012**, *11*, 1675–1678. [CrossRef]
13. Huang, C.; Kawajiri, T.; Ishikuro, H. A 13.56-MHz Wireless Power Transfer System With Enhanced Load-Transient Response and Efficiency by Fully Integrated Wireless Constant-Idle-Time Control for Biomedical Implants. *IEEE J. Solid-State Circuits* **2018**, *53*, 538–551. [CrossRef]
14. Xu, Q.; Hu, Q.; Wang, H.; Mao, Z.-H.; Sun, M. Optimal Design of Planar Spiral Coil for Uniform Magnetic Field to Wirelessly Power Position-Free Targets. *IEEE Trans. Magn.* **2021**, *57*, 4000709. [CrossRef]

15. Chang, H.; Lim, T.; Lee, Y. Compensation for lateral misalignment in Litz wire based on multilayer coil technology. *Sensors* **2021**, *21*, 2295. [CrossRef] [PubMed]
16. Wang, M.; Li, M.; Luo, Q.; Shi, Y. Capacitance Prediction Using Multicascade Convolutional Neural Network for Efficient Wireless Power Transfer. *IEEE Antennas Wirel. Propag. Lett.* **2024**, *23*, 3822–3826. [CrossRef]
17. *IEEE Std C95.1-2019 (Revision of IEEE Std C95.1-2005/Incorporates IEEE Std C95.1-2019/Cor 1-2019)*; IEEE Standard for Safety Levels with Respect to Human Exposure to Electric, Magnetic, and Electromagnetic Fields, 0 Hz to 300 GHz. IEEE: Piscataway, NJ, USA, 2019.
18. Ahmad, A.; Choi, D.-Y. Efficient Metamaterial-Integrated Radiative Near-Field Wireless Power Transfer System for Scalp-Implantable Devices in IoMT Applications. *IEEE Internet Things J.* **2025**, *12*, 25879–25891.
19. Dai, Z.; Sun, Y.; Gan, Q.; Zhai, Y.; Wang, H.; Wei, X.; Ye, S.; Zhang, M.; Sun, M.; Song, J.; et al. Hybrid Wireless Power Transfer With Self-Resonance Coupler Based on Integrated Coil. *IEEE Trans. Power Electron.* **2026**, *41*, 7030–7040.
20. Zhao, H.; Tian, Z.; Zhang, X.; Qiu, Y.; Li, L.; Chen, P.; Yang, F.; Wu, X.; Xu, G. Nonresonant Compensation Optimization for Efficiency Improvement of Wireless Power Transfer System With Relay Coil. *IEEE Trans. Power Electron.* **2024**, *39*, 2835–2845.
21. Zhuang, H.; Wang, W.; Yan, G. Omnidirectional Wireless Power Transfer System Using Modified Saddle-Shaped Coil Pair for Implantable Capsule Robots. *IEEE Trans. Power Electron.* **2023**, *38*, 11664–11672. [CrossRef]
22. Roy, S.; Azad, A.N.M.W.; Baidya, S.; Alam, M.K.; Khan, F. Powering Solutions for Biomedical Sensors and Implants Inside the Human Body: A Comprehensive Review on Energy Harvesting Units, Energy Storage, and Wireless Power Transfer Techniques. *IEEE Trans. Power Electron.* **2022**, *37*, 12237–12263. [CrossRef]
23. Qin, R.; Costinett, D. Review of Self-Resonant Coils for Wireless Power Transfer. *IEEE Access* **2025**, *13*, 190590–190617. [CrossRef]
24. Zhu, H.; Wu, X.; Xiong, F.; Tahir, M. Robust Wireless Power and Data Transmission System against Misalignment for Implantable Medical Devices. *IEEE Trans. Power Electron.* **2025**, *40*, 14169–14180. [CrossRef]
25. Jayathurathnage, P.; Liu, Y.; Kyyrä, J. Self-Decoupled and Integrated Coils for Modular Multitransmitter Wireless Power Transfer Systems. *IEEE Trans. Power Electron.* **2022**, *37*, 12962–12967. [CrossRef]
26. Han, D. Stable Wireless Power Transfer System for Capsule Robot Using Three-Dimensional Hybrid Transmitting Coil Pairs. *IEEE Trans. Power Electron.* **2025**, *40*, 8824–8833. [CrossRef]
27. Huh, S.; Park, B.; Choi, S.; Shin, Y.; Kim, H.; Kim, J.; Park, J.; Park, D.; Ahn, S. Transmitter Coils Selection Method for Wireless Power Transfer System with Multiple Transmitter Coils and Single Receiver Coil. *IEEE Trans. Power Electron.* **2023**, *38*, 4092–4109. [CrossRef]
28. Li, Y.; Feng, Y.; Guo, Y. Triangulated Transmitter Coils with High Design Freedom for Free-Positioning and Omnidirectional Wireless Power Transfer System. *IEEE Trans. Power Electron.* **2025**, *40*, 2619–2629.
29. Niu, S.; Liu, W.; Liu, C.; Jia, C.; Liserre, M.; Chau, K.T. A non-intrusive integration of wireless chargers into electric vehicles: 95.60% dc-dc efficiency at 0.51 LD-to-CL ratio with on-vehicle demonstration. *eTransportation* **2026**, *27*, 100547. [CrossRef]
30. *IEEE Std 802.15.6-2012*; IEEE Standard for Local and Metropolitan Area Networks—Part 15.6: Wireless Body Area Networks. IEEE: Piscataway, NJ, USA, 2012; pp. 1–271. [CrossRef]

Disclaimer/Publisher's Note: The statements, opinions and data contained in all publications are solely those of the individual author(s) and contributor(s) and not of MDPI and/or the editor(s). MDPI and/or the editor(s) disclaim responsibility for any injury to people or property resulting from any ideas, methods, instructions or products referred to in the content.